Design and Simulation of A Novel Highly Symmetrical Piezoelectric Triaxial Accelerometer

Gang Li*, Zhihong Li, Congshun Wang, Yilong Hao, Ting Li, Guoying Wu
Institute of Microelectronics, Peking University, Beijing 100871, P. R. China
Tel: 86-10-62752536, Fax: 86-10-62751789, *Email: ligang@ime.pku.edu.cn

ABSTRACT

A monolithic piezoelectric triaxial accelerometer, using a highly symmetric quad-beam structure with a single seismic mass, has been developed. The structure of the accelerometer is analyzed in detail theoretically and numerically. Static and modal simulations with FEM (Finite Element Method) simulator are done to analyze mechanical response at different applied accelerations. The simulated results show that the accelerometer can sense triaxial acceleration separately simultaneously. It has sensitivities about 21*mV/g*, 15*mV/g* and 15*mV/g* in *Z*-, *X*- and *Y*-axis, respectively. Moreover, nearly zero cross-axis sensitivity can be obtained theoretically. Some design optimizations are done to improve its performance.

Keywords: triaxial accelerometer, piezoelectric, quad-beam, zero cross-axis sensitivity

INTRODUCTION

Micromachined accelerometer is very attractive for space navigation and automobile applications, such as airbag and automatic guidance, because of its size, weight, cost and power advantages. In some applications, such as guidance and sophisticated motion control systems, triaxial accelerometers are needed to sense acceleration in three directions. In this paper, a monolithic piezoelectric triaxial accelerometer, which has only one seismic mass, is designed and simulated. Then it is compact, compared with the device that has three seismic masses [1]. It is predicted to have nearly zero cross-sensitivity, good linearity, high sensitivity and good temperature performance. Besides, some design optimizations are done to improve its performance.

THEORY AND SENSOR DESIGN

It is well known that the triaxial accelerometer requires very low cross-axial sensitivity and good linearity. Besides, close sensitivities in three directions are also expected. To meet these needs, a highly symmetric quad-beam structure [2] is chosen.

First, the operating principle of the device is discussed. A schematic drawing of the accelerometer is shown in Figure 1. The accelerometer consists of a seismic mass and four beams suspending the seismic mass.

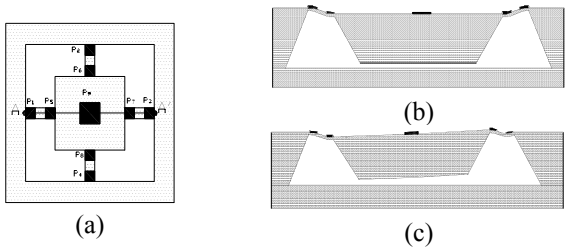

Figure1: Schematic drawing and operating principle of our accelerometer:
(a) Top view;
(b) Vertical acceleration applied;
(c) Horizontal acceleration applied.

For our device, the change of the beam stress, caused by acceleration, is detected by piezoelectric cells. When the acceleration is applied on the mass, it causes the beam to bend and produces strain in piezoelectric thin film. The piezoelectric effect converts the strain into an electrical charge that is proportional to the acceleration (assuming small deflections).

A piezoelectric cell is taken as a piezoelectric capacitor equivalently. The bottom surfaces of all piezoelectric cells are connected together, shown in Figure 2. C_1~C_9 are corresponded to the capacitance of piezoelectric cells P_1~P_9, respectively. C_1~C_8 have the same capacitance, assumed to equal C_0. C_9 is four times larger than the others, namely $C_9=4C_0$. C_9 is an unstrained compensatory capacitor, used to cancel the pyroelectric common mode signal. Piezoelectric cells P_1 and P_3, P_2 and P_4, P_5~P_9 are used to sense *X*-, *Y*- and *Z*-axis acceleration respectively, shown in Figure 2. Besides, $V_x=(Q_1-Q_3)/C_0$, $V_y=(Q_2-Q_4)/C_0$ and $V_z=(Q_5+Q_6+Q_7+Q_8)/4C_0$ respectively, where Q_1~Q_8 are the electric charge signal caused by stress on piezoelectric cells P_1~P_8 respectively.

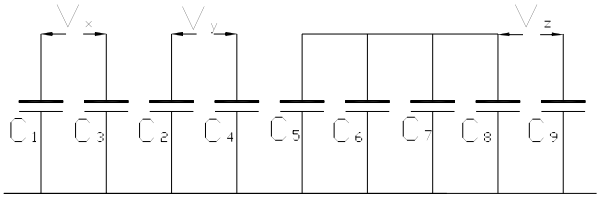

Figure 2: Equivalent circuit for the accelerometer.

Table 1: Electric charge change at different direction accelerations.

	Q_1	Q_2	Q_3	Q_4	Q_5	Q_6	Q_7	Q_8	Q_9	V_x	V_y	V_z
a_x	-	*0*	+	*0*	+	*0*	-	*0*	*0*	$2Q_1/C_0$	*0*	*0*
a_y	*0*	+	*0*	-	*0*	-	*0*	+	*0*	*0*	$2Q_2/C_0$	*0*
a_z	-	-	-	-	+	+	+	+	*0*	*0*	*0*	Q_5/C_0

+, Positive value; -, Negative value; *0*, Cancelled or unchanged.

When the seismic mass is accelerated vertically (Figure 1(b)), it translates down along *Z*-direction. It causes a symmetric stress distribution in the beams. It produces tensile stress in piezoelectric cells P_1~P_4 and compressive stress in piezoelectric cells P_5~P_8. Consequently, it produces negative electric charge signal in piezoelectric cells P_1~P_4 and positive electric charge signal in piezoelectric cells P_5~P_8. Therefore, the differential voltage signal V_z, which is not equal zero, can be obtained. However, V_x and V_y all equal zero because Q_1~Q_4 are all common mode signal.

When the seismic mass is subjected to a lateral acceleration in the *X*-direction, it rotates around *Y*-axis because the center of the mass is not in the plane of the suspension beams. It causes an antisymmetric stress distribution in the beams and piezoelectric thin film. It produces tensile stress in piezoelectric cells P_1, P_7 and compressive stress in piezoelectric cells P_3, P_5. It also causes shear stress in P_2, P_4, P_6 and P_8, which are small enough to be neglected because the beam is much wider than thick. Consequently, it produces negative electric charge signal in piezoelectric cells P_1, P_7 and positive electric charge signal in piezoelectric cells P_3, P_5. Therefore, the differential voltage signal V_x, which is not equal zero, can be obtained. However, V_y equals zero because Q_2, Q_4 are common mode signal and V_z~*0*, because Q_5, Q_7 are differential signal which cancels out each other and Q_6, Q_8 are very small.

Because this structure is symmetric in *X*- and *Y*-direction, the results derived from *X*-direction are fit for *Y*-direction and vice versa.

To describe the relations clearly, the behavior of electric charge change at different accelerations is summarized in Table 1. From Table 1, it is obvious that piezoelectric cells P_1 and P_3, P_2 and P_4, P_5~P_9 are used to sense *X*-, *Y*- and *Z*-axis acceleration separately.

In addition, the device is expected to have good temperature performance because the pyroelectric effects are common mode signal, which is canceled in the device.

FEM SIMULATION

We testify our device with a FEM (Finite Element Method) simulation program *ANSYS* release 5.4. The FEM simulations of modal and static analysis are very useful for our design. The beam length, width and thickness are 300, 100 and 5 μm respectively. The top surface area and the thickness of the seismic mass are 1500_1500 μm^2 and 400 μm respectively. The top surface area of the piezoelectric cells P_1~P_8 and P_9 are 100_100 μm^2, respectively. The thickness of all piezoelectric cells is 0.5 μm.

The results of modal simulation are listed in Table 2.

Table 2: Modal simulation results.

Resonance frequency [Hz]	1st mode : 2444
	2nd mode : 3744
	3rd mode : 3745
	4th mode : 70951

The first three modes correspond to *Z*-direction translation and *X*-, *Y*-direction rotation respectively. From Table 2, it is obvious that the frequencies of the first three modes are close to each other, which meets the need of close sensitivities in three directions. Moreover, the frequency of the fourth mode is much larger than the ones of the first three modes, which is favorable for the performance against disturbance.

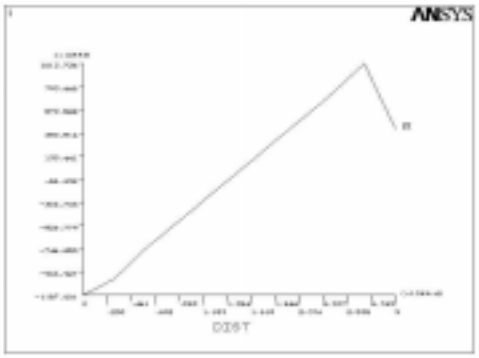

Figure 3: The stress distribution of one beam under *1g Z*-axis acceleration.

Figure 3 shows stress distribution of one beam when only *Z*-direction acceleration is applied on seismic mass. It is found that the maximum stress mainly concentrates on the both ends of the beam. Therefore, piezoelectric cells are arranged at the both ends of each beam. We also have checked the translation of the seismic mass along *Z*-direction when an *1g Z*-direction is acted on it. It is only found 4.15×10^{-2} μm displacement that is small enough, compared with beam thickness, to guarantee the good linearity of our device.

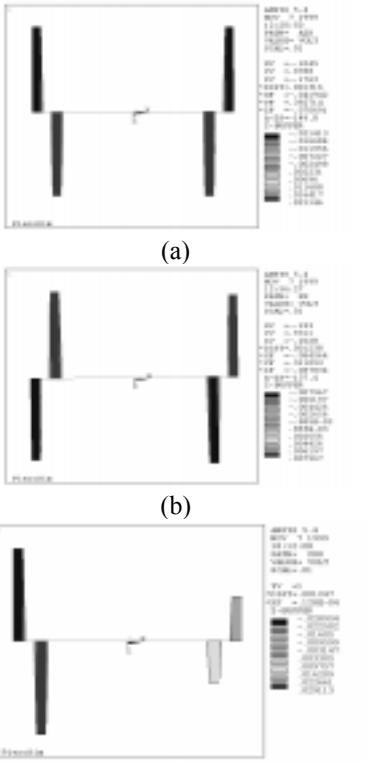

Figure 4: The voltage distribution from one end of the beam, across the seismic, to the end of the opposite beam.
(a) The displacement when an *1g Z*-direction acceleration is applied.
(b) The displacment when an *1g X*-direction acceleration is applied.
(c) The displacment when an *1g X*- and *Z*-direction acceleration is applied.

Using multi-physics coupling analysis, the simulated results of the voltage distribution on the path *AA'* (Figure 1 (a)) are obtained in Figure 4, when a vector acceleration is applied on the seismic mass. Figure 4 (a), (b), (c) illustrate that the seismic mass translates along *Z*-direction, rotates along *Y*-axis, translates and rotates when a *Z*-, *X*-direction acceleration applies on it separately and simultaneously, respectively. The voltage value of the down surface of each piezoelectric cell is defined to 0 *V*. We also couple the voltage value of the top surface of each piezoelectric cell together, so it produces the average voltage.

To get straightforward results, the voltage of each piezoelectric cell (shown in Figure 1 (a)) in the different accelerations is listed in Table 3. From Table 3_ it is obvious that the results of the static simulation of the device accord our thought well and the device has sensitivities about 21 *mV/g*, 15 *mV/g* in *Z*- and *X*-axis respectively. Nearly zero cross-axis sensitivity can also be gained.

Because this structure is symmetric in *X*- and *Y*-direction, the results derived from *X*-direction are fit for *Y*-direction and vice versa.

The mechanical performance can be improved by optimizing structure shapes of the seismic mass and/or beam.

First, the new seismic mass shape is used to improve sensitivity in the same die size of our device. The new seismic mass shape is shown in Figure 5. In this case, volume of the seismic mass is increased without changing die size.

Secondly, the beam shapes are optimized to get better performance. Three types of the beams, which are illustrated in Figure 6, are simulated. The beam length and thickness is 300 μm and 5 μm respectively. The beam width varies in the beam length direction. Figure 7 shows the stress and displacement of the three beams when they are applied on an 1×10^{-6} *N* force. From Figure 7, it is obtained that the displacement of beam 3 is the smallest while the maximum stress of all beams are approximately same. It means that the accelerometer suspended by beam 3 has better linearity and has the same sensitivity compared with other types of beams when other parameters are same.

CONCLUSION

A monolithic piezoelectric triaxial accelerometer is designed and simulated, using FEM program *ANSYS*. It is found that the design is feasible and the device has sensitivities about 21*mV/g*, 15*mV/g* and 15*mV/g* in *Z*-, *X*- and *Y*-axis, respectively. Moreover, nearly zero cross-axis sensitivity can be obtained theoretically. Some design optimizations are done to improve its performance. Additionally, the fabrication process and test results will be discussed in the future related issues.

Table 3: The voltage of each piezoelectric cell in the different accelerations.

	V_{P1}	V_{P2}	V_{P3}	V_{P4}	V_{P5}	V_{P6}	V_{P7}	V_{P8}	V_x	V_y	V_z
a_z=*1g*	-21.4	-21.4	-21.4	-21.4	21.1	21.1	21.1	21.1	0	0	21.1
a_x=*1g*	-7.5	-7e-8	7.5	8e-8	7.97	8e-8	-7.97	-9e-8	-15	-1.5e-7	-1e-8
a_z=a_x=*1g*	-28.9	-21.4	-13.9	-21.4	29.1	21.1	13.1	21.1	-15	0	21.1

*Note: The voltage unit is *mV*.

REFERENCES

1. Patrick Scheeoer, Jens Ole Gullov and Lars Munch Kofoed, A piezoelectric triaxial accelerometer, Journal of Micromech. Microeng. 6 (1996) pp. 131-133.
2. R. P. Van Kampen and R. F. Wolffenbuttel, Modeling the mechanical behavior of bulk-micromachined silicon accelerometers, Sensors and Actuators A 64 (1998) 137-150.

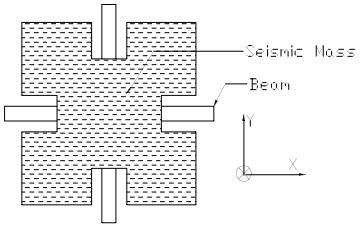

Figure 5: Top view of the reformative geometric shape of seismic mass.

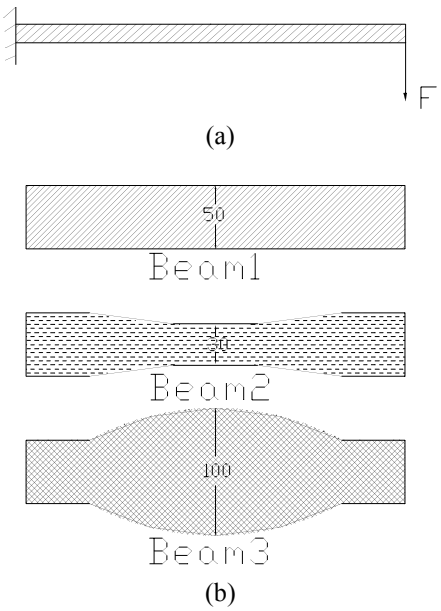

Figure 6: The shape of the three kind of beams.
(a) Cross section of the beams.
(b) Top view of the shape of the beams.

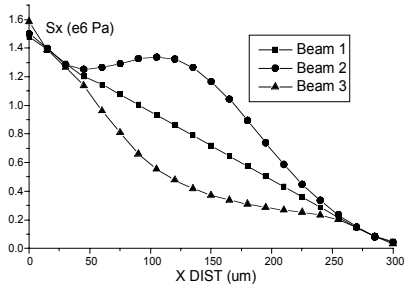

(a)

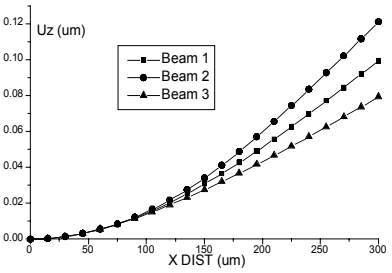

(b)

Figure 7: The stress and displacement distribution of the three beams.
(a) The stress distribution.
(b) The displacement distribution.